MODELLING AND IMPLEMENTATION OF A PERMANENT MAGNET SYNCHRONOUS MOTOR DRIVE USING A DSP DEVELOPMENT ENVIRONMENT

S. Van Haute, G. Terörde, K. Hameyer, R. Belmans

Katholieke Universiteit Leuven, Belgium

Abstract. A permanent magnet synchronous motor drive using a prototype 6 pole 3 kW inset magnet motor is presented. The drive is controlled by a DSP based control board that can be programmed using the MATLAB®/SIMULINK® software. To investigate the influence of saturation, an accurate measurement procedure based on load tests is described. This method benefits from the I/O features of the development environment. The theoretical performance limits of the motor are determined using optimal torque control. Finally, aspects of controller design, simulation and implementation are briefly discussed.

Keywords. Permanent magnet synchronous motor, flux-weakening, digital control, DSP, d/q-modelling.

INTRODUCTION

With the introduction of permanent magnets with a high flux density as well as a high coercivity in the late eighties, synchronous motors with permanent magnets became an attractive alternative for application in high performance variable speed drives. In the power range of a few kW to several tens of kW, the sinusoidal excited permanent magnet synchronous motor (PMSM) is preferred. It has better characteristics than the brushless DC motor with square wave currents, especially when a large constant power operation is required. Furthermore, advantage can be taken of the additional reluctance torque when direct and quadrature reactances have different values. In designs with inset and interior magnets, usually X_d is smaller than X_q.

In this paper, a motor drive with a prototype PMSM with inset magnets and flux weakening capabilities is described. As the magnetic parameters of inset and interior PMSMs depend on the saturation level, an accurate measurement procedure based on load tests is developed. The results are compared to numerical calculations from a finite element model. For the prototype motor, the theoretical maximum performance over the entire speed range is determined. For the instantaneous torque control, a commercially available DSP based environment is used. A standard VSI-PWM invertor with IGBTs is adapted to be commanded by the DSP control board.

PERMANENT MAGNET SYNCHRONOUS MOTOR MODEL

Permanent magnet synchronous motors are usually modelled in the rotor reference frame, i.e. Park's d-q model. In this synchronous reference frame, the PMSM without rotor damper cage is generally described by the following set of equations.

$$u_d = Ri_d + L_d \frac{\mathrm{d}i_d}{\mathrm{d}t} - \omega L_q i_q \tag{1}$$

$$u_q = Ri_q + L_q \frac{\mathrm{d}i_q}{\mathrm{d}t} + \omega L_d i_d + \omega \psi_{Md} \tag{2}$$

where ω is the electrical angular speed and ψ_{Md} is the permanent magnet flux. The electromechanical torque can be expressed as follows:

$$T_e = p\left[\psi_{Md} i_q - \left(L_q - L_d\right) i_d i_q\right] \tag{3}$$

This model neglects rotor damping and iron losses. However, it can be adapted to take stator iron losses into account [1],[2].

The prototype motor used in the simulation and experiments is a 3 kW permanent magnet synchronous motor with sinusoidal currents. Figure 1 shows the layout of the rotor. This motor type is referred to as a *surface-inset* PMSM [3] and combines some advantages of both surface mounted and interior permanent magnet motors. From the rotor geometry it can be seen that the direct axis inductance L_d is smaller than the quadrature axis inductance L_q. This results in an additional reluctance torque as indicated in equation (3) and allows for maximum torque-per-Ampere control and an extended flux weakening range [4]. The phasor diagram for motor operation is shown in figure 2. The phasor diagram represents a stationary regime, hence effective values for currents and voltages are used (indicated by capitals).

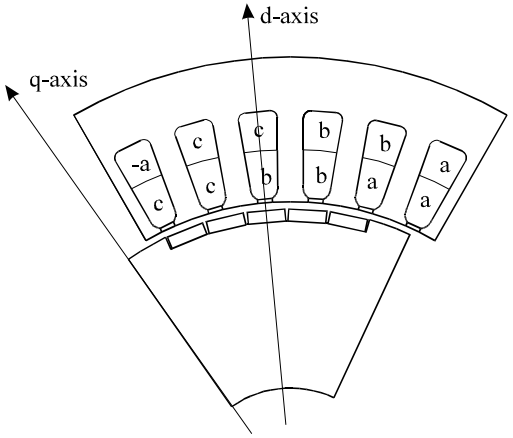

Figure 1 Stator and rotor geometry of the 6-pole prototype inset PMSM with the rotor d-axis aligned with the magnetic axis of the reference stator phase.

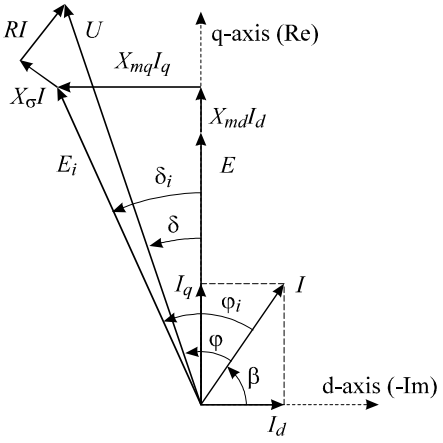

Figure 2 Phasor diagram of a PMSM.

DETERMINATION OF MAGNETIC PARAMETERS AND INFLUENCE OF SATURATION

The optimal control of permanent magnet synchronous motors requires the accurate knowledge of the machine parameters. Generally, the magnetic parameters depend on the saturation level. For machines with interior magnets, all magnetic parameters (L_d, L_q and ψ_M) show a significant variation with load current [2]:

- L_d (i_d);
- L_q (i_q);
- ψ_M (i_q).

Due to saturation, also interaction between d-axis and q-axis (cross-coupling) can occur [5], however, these can be considered as second order effects [6],[2]. Moreover, for the inset magnet type PMSM, only an important variation of L_q with i_q is expected.

Several methods for measuring the d/q inductances of permanent magnet machines at different current and thus saturation levels have been reported in literature [2],[7],[8]. They can be classified in three categories:

- static tests;
- load tests without load angle measurement;
- load tests with load angle measurement.

Static Tests

In [2] it is shown how the parameters for different load currents can be obtained combining static and no-load tests, without measuring the load angle. However, this requires the use of a special inductance bridge operating with a DC voltage. As an alternative, it is investigated here if L_d and L_d can be determined accurately from the phase inductances. With an ordinary inductance bridge, the phase inductance values are measured directly at the machine terminals for different rotor positions (figure 3).

The d/q machine model is based on a sinusoidal variation of the inductance values. Therefore, a Fourier transform is performed and only the constant value and the first harmonic are taken into account (figure 4).

According to figure 4, the d/q inductances can be written as

$$L_d = L_\sigma + \frac{3}{2}\left(L'_0 - L_2\right) \tag{4}$$

$$L_q = L_\sigma + \frac{3}{2}\left(L'_0 + L_2\right) \tag{5}$$

The leakage inductance can not be separately determined from experiments. As a consequence, the d/q inductance values can only be approximated as

$$L'_d = \frac{3}{2}L_{0°} \tag{6}$$

$$L'_q = \frac{3}{2}L_{90°} \tag{7}$$

It can be shown that the theoretical error is of the order of half the leakage inductance.

A second method to determine L_d and L_d from static tests is based on the d/q transformation matrix equation.

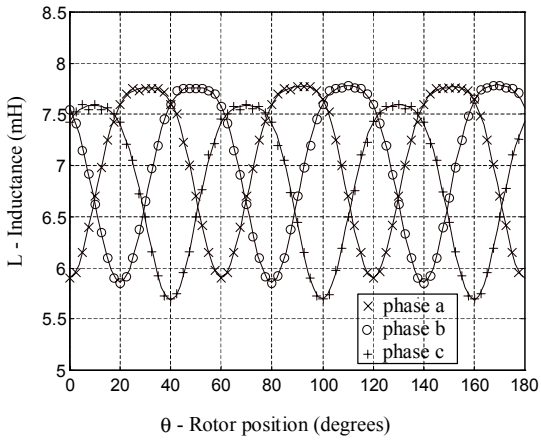

Figure 3 Measured phase inductance values as function of rotor position for the motor shown in figure 1.

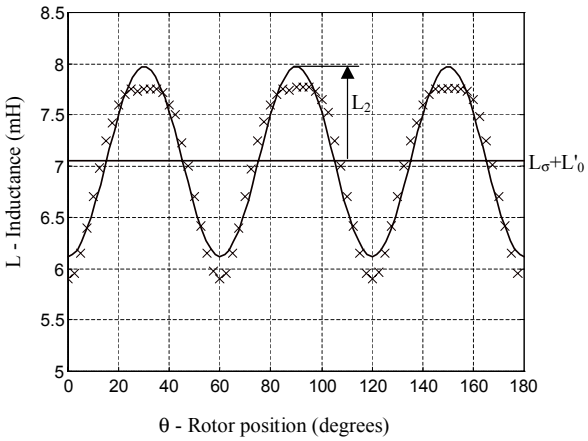

Figure 4 Measured values, constant value and first harmonic of the phase inductance value as function of rotor position.

$$\mathbf{L}_{dq} = \mathbf{T}_\theta \left(\mathbf{T}_{32} \mathbf{L} \mathbf{T}_{23} \right) \mathbf{T}_\theta^{-1} = \begin{bmatrix} L_d & 0 \\ 0 & L_q \end{bmatrix} \tag{8}$$

with **L** the stator inductance matrix

$$\mathbf{L} = \begin{bmatrix} L_{aa} & L_{ab} & L_{ac} \\ L_{ba} & L_{bb} & L_{bc} \\ L_{ca} & L_{cb} & L_{cc} \end{bmatrix} \tag{9}$$

For an arbitrary rotor position, the three phase inductance values are measured, as well as the inductance of two phases in series.

$$L_{ab} = -\frac{1}{2}\left(L_{abs} - L_{aa} - L_{bb} \right) \tag{10}$$

$$L_{ac} = -\frac{1}{2}\left(L_{acs} - L_{aa} - L_{cc} \right) \tag{11}$$

$$L_{bc} = -\frac{1}{2}\left(L_{bcs} - L_{bb} - L_{cc} \right) \tag{12}$$

The results are summarized in Table 1. There is a relatively large difference for the calculated values for L_d between the applied methods. It can be concluded that the investigated methods give only an idea of the magnitude of the inductances, but are unreliable for accurate modelling the motor.

Load Tests

It has been shown in [Chalmers85] and [Stumberger97] that accurate inductance values from load tests, including the variations due to saturation, can only be obtained after a considerable amount of measurement data processing to reduce the effect of random errors. The procedures described in [Chalmers85] and [Stumberger97] are modified, requiring less measurements and measurement data processing without loosing accuracy. The measurement set-up is shown in figure 5 and uses the same DSP environment as for the control, which is described later in this paper. The machine under test is driven by a DC machine and operates as a generator.

The originality of the procedure lies in the fact that all data necessary to reconstruct the phasor diagram, including the load angle δ, are obtained from the registration of the voltage, the current waveforms and an encoder signals during one or two periods (figure 6). The inductance values are calculated using the fundamental currents and voltages. The data from the digital power analyzer are averaged data over several periods and serve only as a check. Mixing these values with values obtained from the captured waveforms could introduce errors in the final results. Curve fitting to evaluate saturation influence on parameters is only necessary on the final results and not in the intermediate calculation steps, as required in [Stumberger97]. The results for the machine with inset magnets are summarized in Table 2 and Table 3. The recalculated inductances from the measurement data are in general higher than the values obtained from numerical calculations using the flux linkage method [5]. This is because the latter do not include the end winding leakage.

TABLE 1 - d/q inductance values obtained from static tests

Inductance	via directly measured $L_{0°}$ and $L_{90°}$	via $L_{0°}$ and $L_{90°}$ from first harmonic	via inductance matrix
L_d (mH)	8,73	9,04	7,35
L_q (mH)	11,57	11,93	11,99

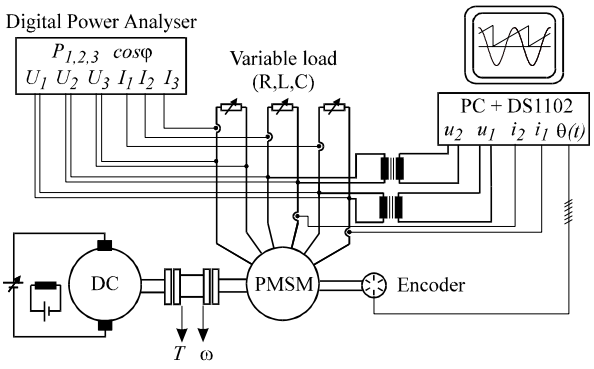

Figure 5 Measurement set up to determine the d/q model inductance values from load tests.

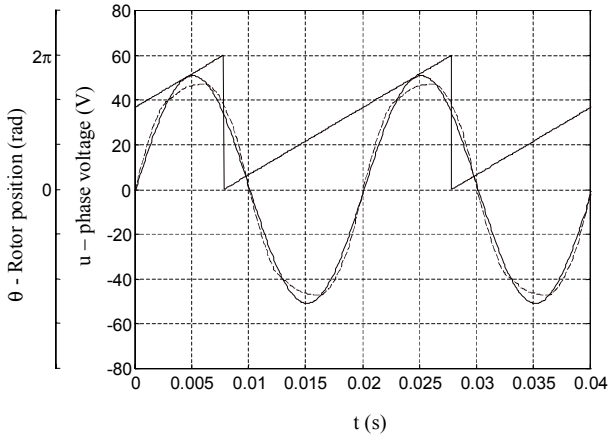

Figuur 6 Rotor position, measured terminal voltage and calculated fundamental voltage for the reference phase of the PMSM (f=50 Hz, 7,6 A, δ=-40,2°).

TABLE 2 - Inductance values and torque calculated from measurements at different currents and load angles.

I (A)	δ (°)	L_d (mH)	L_q (mH)	T_e (Nm)
3,9	-21,5	8,8	14,8	-5,06
5,5	-30,1	8,8	15	-7,12
7,6	-40,2	8,9	15,1	-9,33
8,1	-42,3	9	14,9	-9,73

TABLE 3 - Inductance, load angle and torque values obtained from numerical calculations (inset magnet motor).

I (A)	δ (°)	L_d (mH)	L_q (mH)	T (Nm)
3,9	-21,34	8,43	14,87	-5,04
5,5	-29,44	8,52	14,87	-7,05
7,6	-38,65	8,38	14,88	-9,25
8,1	-40,71	8,36	14,88	-9,68

Theoretical, the difference for L_d and L_q must be identical. However, in Table 2 L_d and L_q are calculated from the measured data which include the effect of stator core losses. Adjusting the phasor diagram [Honsinger98] and recalculating the motor parameters results in slightly higher inductances, with a larger increase in L_q than in L_d.

It can be seen that for this specific prototype motor, the inductances are constant, indicating that the level of saturation in d-axis and q-axis remains constant. However, in [10] it is shown that it can occur that for a similar rotor design, the q-axis inductance decreases as q-axis current increases due to the saturation in the stator. This strongly affects the performance and control of the motor.

PERFORMANCE CHARACTERISTICS USING FLUX WEAKENING

The optimal control of PMSMs with $L_d < L_q$ takes advantage of the reluctance torque by introducing a negative direct axis stator current component. This results in a maximum torque-per-Ampère trajectory in the i_d - i_q plane (figure 7), given by the following equation:

$$i_q^2 = i_d^2 - \frac{\psi_{Md} i_d}{L_q - L_d} \tag{13}$$

For stationary operation, the current is limited by the rated motor current I_r resulting in rated torque The motor voltage is limited by the power electronic inverter. This implies that for a given rotor speed, the current vector must lie within a corresponding boundary. When stator resistance is neglected, this limiting curves are ellipses decreasing in size when rotor speed increases [4].

$$\frac{3}{2}\left(\frac{(2/\pi)U_{DC}}{p\omega_r L_q}\right)^2 \geq i_q^2 + \left(\frac{L_d}{L_q}\right)^2\left(i_d + \frac{\psi_{Md}}{L_d}\right)^2 \tag{14}$$

As a consequence, rated torque can not be maintained above the speed at which the voltage limit ellipse intersects the maximum torque-per-Ampère trajectory. This speed is the base speed of the motor.

$$\omega_{rb} = \sqrt{\frac{3}{2}}\frac{2U_{DC}}{\pi p L_q \sqrt{i_{qb}^2 + \left(\frac{L_d}{L_q}\right)^2\left(i_{db} + \frac{\psi_{Md}}{L_d}\right)^2}} \tag{15}$$

Reducing the current along the maximum torque-per-Ampère trajectory above base speed results in a fast decrease of output torque. As an alternative, the operating point can be forced to leave the maximum torque-per-Ampère trajectory along the current limit circle resulting in further flux weakening at maximum current (figure 7). The high speed operating region is considerably extended using the flux weakening algorithm.

The maximum speed is reached when all stator current is in the direct axis and is given by

$$\omega_{r3} = \sqrt{\frac{3}{2}}\frac{2U_{DC}}{\pi p L_d\left|-\sqrt{3}I_{Nx} + \frac{\psi_{Md}}{L_d}\right|} \tag{16}$$

The maximum speed becomes theoretically infinite when

$$\frac{\psi_{Md}}{L_d} = \sqrt{3}I_N = i_{\max} \tag{17}$$

The factor $\sqrt{3}$ in (17) as well as 3/2 and $\sqrt{3/2}$ in (14), (15) and (16) are due to the use of the power invariant form of the Park transformation.

Introducing the voltage limited maximum power curve, without regarding the current limit [11], the current can be reduced at very high speeds when $\psi_{Md}/L_d < \sqrt{3}I_N$. In this case, the control trajectory yielding maximum output at all speeds is indicated in figure 8. Calculated results for the prototype motor are shown in figure 9. The results are obtained using The motor parameters are summarised at the end of this paper.

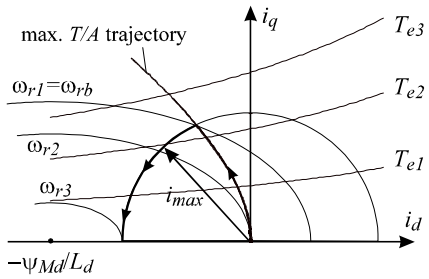

Figure 7 Constant torque hyperbolas, maximum torque-per-Ampère trajectory, current limit circle, voltage limit ellipses and optimum current trajectory when $\psi_{Md}/L_d > i_{max}$.

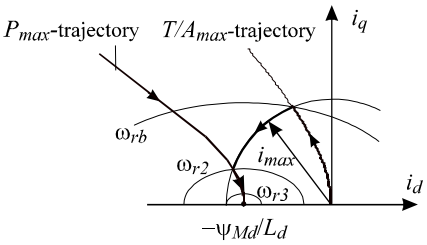

Figure 8 Optimum current trajectory when $\psi_{Md}/L_d < i_{max}$.

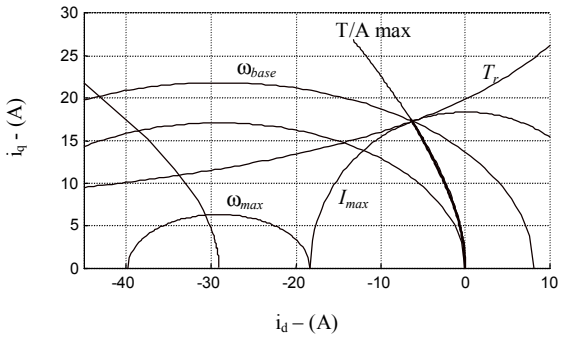

Figure 9 Torque hyperbolas, voltage limit ellipses, current limit circle, maximum power and maximum torque-per-Ampère trajectory for the prototype motor.

EXPERIMENTAL SET-UP

The motor control is implemented using a DSP based controller board with additional I/O features and an encoder interface (dSPACE DS1102). This is a MATLAB®/SIMULINK® based development environment. The laboratory test drive further consists of a host PC for the controller board, an IGBT inverter and the prototype motor , current sensors and an incremental encoder (figure 10).

The heart of the controller board is a TMS320C31 digital signal processor. A slave processor is used to perform the digital input and output signals and generate the PWM signals. The controller board can be directly programmed using MATLAB®/SIMULINK®. Motor currents are measured using LEM sensors and fed to the control board. These signals should be be filtered either analog or digital. Due to the parasitic capacitive currents and the fact that the analog filters can not be placed close to the inputs of the A/D converters, digitally filtering is preferred here. Phase shift introduced by the filter can be corrected if necessary by adapting the transformation angle from the stator to the rotor reference frame. The position is measured using an incremental encoder.

The inverter used is a modified standard VSI-PWM inverter with IGBTs. Only an interface to galvanically isolate the control board from the inverter is added. The PWM switching signals are fed directly from the slave processor to the inverter using a high performance optical link, allowing to keep the inverter and drive several meters from the PC with the control board.

The optimal torque control algorithm determines reference values for direct and quadrature axis currents. The PWM generation scheme implemented in the slave processor is based on phase voltage reference values. Therefore, these reference values are determined using a decoupling network and the inverse Park transformation. Both subharmonic PWM generation as a space vector modulation are implemented.

Figure 10 shows a block scheme of the experimental set-up. The dotted frame indicates the functions implemented on the controller board. The PWM frequency is chosen to be 10 kHz. The current sample period has to be a multiple of the PWM period or can be equal when the DSP can handle the algorithm at that speed.

CONTROLLER DESIGN AND SIMULATION

To design the controllers and simulate the entire drive, it is necessary to take the power electronic converter into account. A power electronic system can be modelled in different ways, or, as often encountered, not modelled at all. The level of modelling to be considered depends on the purpose of the simulation. For control design purposes, the invertor can be simply modelled by a delay. It is shown that for the subharmonic PWM a general delay time of $T_p/3$ is adequate, where T_p is the PWM period [12].

As the drive is controlled by a DSP, it is to be considered as a sampled data system. There are different approaches to model these systems [12], [13]. One possibility is to use a discrete model [14], using the z-transform and to carry out the controller design in the z-domain. To enable the use of frequency response methods, a second transformation is necessary (bilinear transformation). Alternatively, carrying out the initial design using continuous methods can serve as a guide for a direct discrete design. The performance of a system when it could be realised with continuous hardware, is a target for how well the digital system should perform and assists in selecting the sample rate. As shown in [12], under certain conditions a sampled data or discrete system can be treated as a pseudo-continuous system. This has the advantages with respect to the applicability of optimal control formulations. The effect of A/D and D/A converters, as well as the execution time of the control algorithm itself are taken into account by using equivalent continuous transfer functions. The designed optimal controllers can be directly converted to their discrete equivalents.

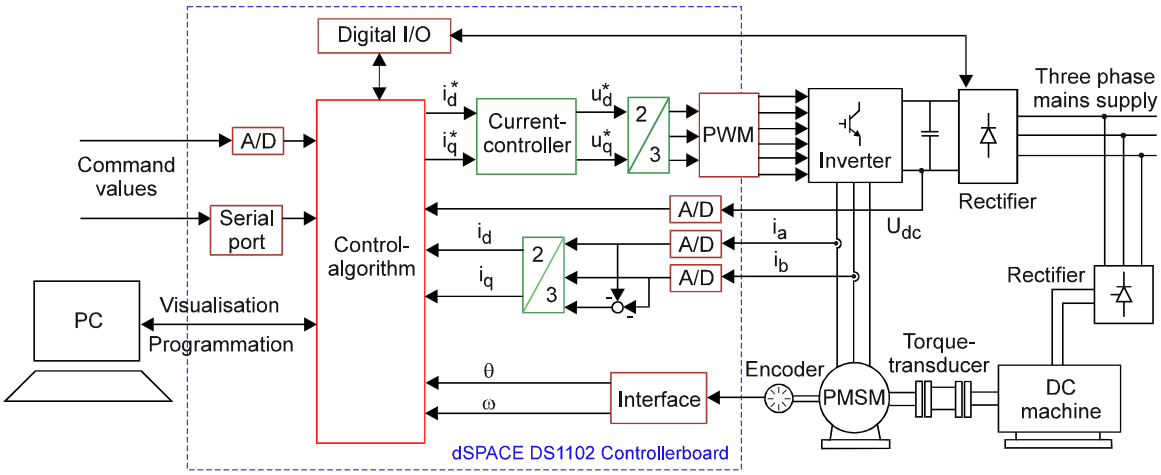

Figure 10 Experimental set-up. Functions implemented on the DSP-control board are indicated by the dashed line.

Simulations of the drive are performed using MATLAB®/SIMULINK®. Classical controllers, i.e. PID are used for the drive. Combined with the pseudo-continuous modelling, this has the advantage that well-known optimisation criteria can be applied.

CONCLUSIONS

A permanent magnet excited synchronous motor drive is presented, using a inset magnet 6-pole prototype motor with $L_d < L_q$. Methods to experimentally determine the d/q magnetic parameters from both static and load tests are investigated. The results from static tests have shown to be rather inaccurate. The best results are obtained using load tests with simultaneous registration of phase voltages, currents and rotor position and reconstruct the phasor diagram using the fundamental values. The theoretical limits of the drive considering rated motor current and voltage inverter limit are resumed. The optimal torque control is implemented using a MATLAB®/SIMULINK® based DSP development environment, using an optic fiber link to control the IGBT inverter. Various PWM algorithms can be programmed. Finally, aspects of modelling a sampled data system and designing the controllers using both continuous and discrete methods are discussed..

Appendix

PROTOTYPE PMSM DATA		
Number of poles	$2p$	6
Power	P	3 kW
Rated speed	n_r	1930 rpm
Rated current	I_r	10,6 A
Rated torque	T_r	15,3 Nm
Stator resistance	R	0,76 Ω
d-axis inductance	L_d	8,8 mH
q-axis inductance	L_d	15 mH
Magnet flux	ψ_{Md}	0,256 Vs

Acknowledgements

The research is supported by Flanders' Secretary of Economy. The authors are also grateful to the Belgian “Fonds voor Wetenschappelijk Onderzoek Vlaanderen” for its financial support of this work and the Belgian Ministry of Scientific Research for granting the IUAP No. P4/20 on Coupled Problems in Electromagnetic Systems. The research Council of the K.U.Leuven supports the basic numerical research.

BIBLIOGRAPHY

[1] Honsinger, V.B.: Performance of polyphase permanent magnet machines. *IEEE Trans. Power Apparatus and Systems*, 99, 1980, 1510-1518.

[2] Mellor, P.H., Chaaban F.B., Binns, K.J.: Estimation of parameters and performance of rare-earth permanent-magnet motors avoiding measurement of load-angle. *IEE Proceedings-B*, 138, 1991, 322-330.

[3] Sebastian, T., Slemon, G.R.: Operating limits of inverter driven permanent magnet motor drives. *IEEE Trans. Industry Applications*, 23, 1987, 327-333.

[4] Jahns, T.M., Kliman, G.B., Neumann, T.W.: Interior permanent magnet synchronous motors for adjustable speed drives. *IEEE Trans. Industry Applications*, 22, 1986, 738-747.

[5] Sneyers, B., Novotny, D.W. Lipo, T.A.: Field weakening in buried permanent magnet AC motor drives. *IEEE Trans. on Industry Applications*, 21, 1985, 398-407.

[6] Chalmers, B.J.: Influence of saturation in brushless permanent-magnet motor drives. *IEE Proceedings-B*, 139, 1992, 51-52.

[7] Chalmers, B.J., Hamed, S.A. Baines, G.D.: Parameters and performance of a high-field permanent-magnet synchronous motor for variable-frequency operation. *IEE Proceedings-B*, 132, 1985, 117-124.

[8] Štumberger, B., Kreca, B. Hribernik, B.: Determination of parameters of synchronous motor with permanent magnets from measurement of load conditions. *IEEE-Int. Electric Machines and Drives Conf. Record, 1997,* WB2-1.1-1.3.

[9] Pahner U., *A general design tool for numerical optimisation of electromagnetic devices*, Ph.D. Thesis, K.U.Leuven, Belgium, 1998.

[10] Van Haute, S., Henneberger, St., Hameyer, K., Belmans, R., De Temmerman, J., De Clercq, J.: Design and control of a permanent magnet synchronous motor drive for a hybrid electric vehicle. Proc. EPE Conf., 1997, 1570-1575,

[11] Morimoto, S., Takeda, Y. Hirasa, T. Taniguchi, K.: Expansion of operating limits for permanent magnet motor by current vector control considereing inverter capacity. *IEEE Trans.Industry Applications*, 26, 1990, 866-871.

[12] Bühler H., *Réglage de systèmes d'électronique de puissance.* Presses polytechniques et universitaires, Lausanne, 1997

[13] Franklin, G.F., Powell, J.D., Workman, M.L.: Digital control of dynamic systems. Second edition, Addison-Wesley, New York, 1990.

[14] Labrique, F., Fu, Y Sente, P. Buyse, H.: Discrete modelling of the field oriented control system in VSI fed AC motor drives,. Proc. *ELECTRIMACS,* 1996, 285-290.

Adress of the authors: Katholieke Universiteit Leuven,
E.E. Dept., ESAT/ELEN
Kardinaal Mercierlaan 94
B-3001 Leuven, Belgium

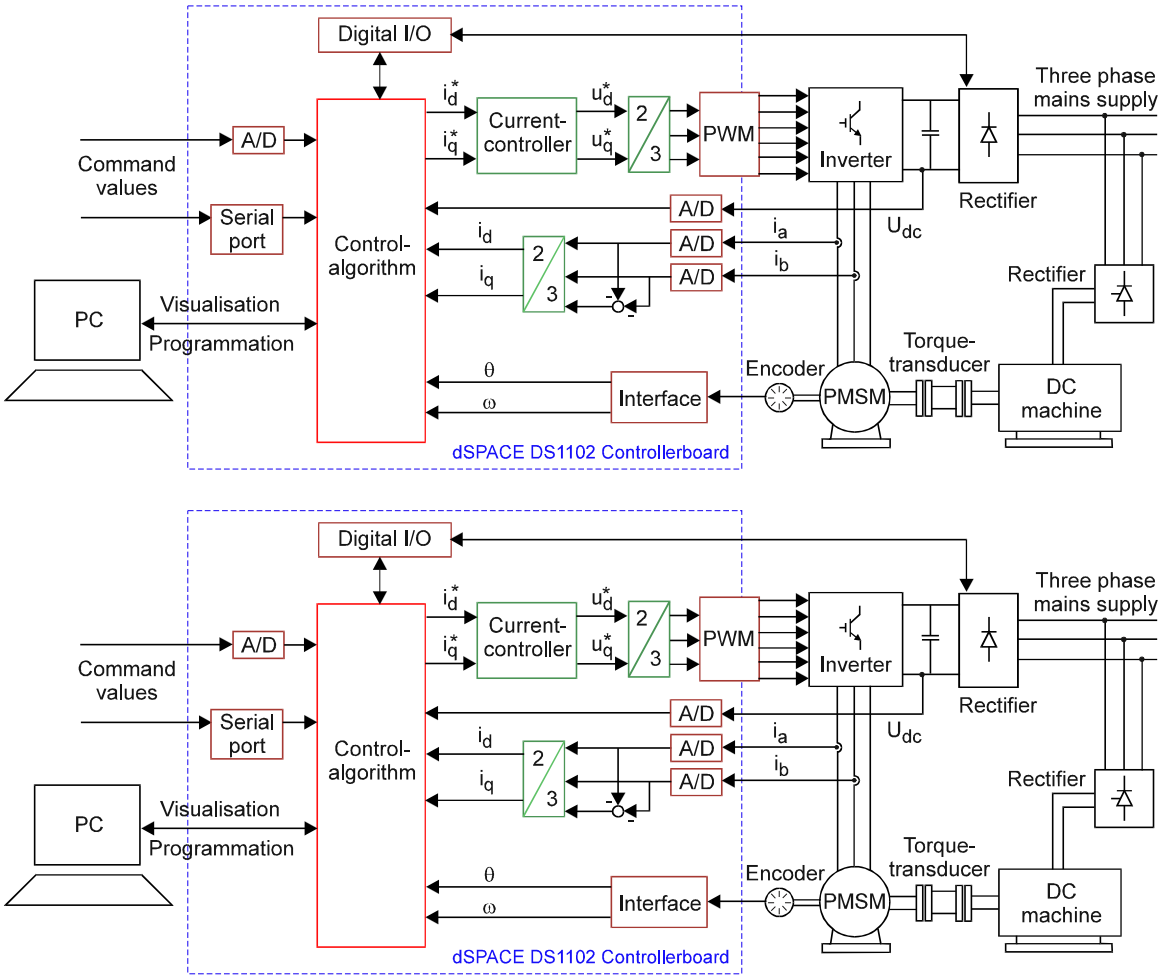

References

1. Binns K.J.; Sneyers B.; Maggetto G.; Lataire Ph.: Rotor-position-controlled permanent magnet synchronous machines for electrical vehicles, ICEM '80, 1980, pp. 346-357.

2. Sneyers B.; Maggetto G.; Van Eck J.L.: Inverter fed permanent magnet synchronous motor road electric traction, ICEM 1982, 1982, pp. 550-553.

3. Jahns T.M.; Kliman G.B.; Neumann T.W.: Interior permanent magnet synchronous motors for adjustable -speed drives, IEEE Transactions on Industry Applications, Vol. IA-22,No.4, 1986, pp.738-747.

[5] Jahns T.M.; Kliman G.B.; Neumann T.W., "Interior permanent magnet synchronous motors for adjustable -speed drives", *IEEE Transactions on Industry Applications,* Vol. IA-22, No.4, 1986, pp.738-747.

4. Morimoto, S.; Sanada, M.; Takeda, Y.: Optimum Machine Parameters and Design of Inverter-Driven Synchronous Motors for Wide Constant Power Operation, Proc. IAS'94, pp. 177-182.

5. Chang, L.; Dawson, G.E.; Eastham, T.R.: Permanent Magnet Synchronous Motor Design: Finite Element and Analytical Methods; ICEM '90, 1990, pp. 1082-1088.

6. Slemon, G. R.; Xian, L.: Modelling and Design Optimisation of Permanent Magnet Motors, Electric Machines and Power Systems, vol. 20, no. 2, 1992, pp. 71-92;

7. Nipp, E.: Alternative to Field Weakening of Surface Mounted Permanent Magnet Motors for Variable Speed Drives, Proc. IAS'95, pp. 191-198.

8. Zhong L.; Rahman M.F.; Lim K.W.: Modelling and experimental studies of an instantaneous torque and field weakening control scheme for an interior permanent magnet synchronous motor drive**,** ELECTRIMACS 1996, pp. 297-302.

9. Nasar, S. A.; Boldea, I.; Unnewehr, L.E.: "Permanent Magnet, Reluctance, and Self-Synchronous Motors", CRC Press, London Tokyo, 1993.

10. Sebastian T.; Slemon G.R.: Operating limits of inverter-driven permanent magnet motor drives, IEEE Transactions on Industry Applications, Vol. IA-23,No.2, 1987, pp. 327-333.

11. Jahns T.M.: Flux-weakening regime operation of an interior permanent-magnet synchronous motor drive, IEEE Transactions on Industry Applications, Vol. IA-23, No.4, 1987, pp.681-689.

12. Hadji-Minaglou J.-R: Antriebskonzepte mit permanent-erregten Synchronmotoren für den Einsatz im Elektrofahrzeug, PhD-thesis RWTH Aachen, 1994.

13. Sneyers B.; Novotny D.W.; Lipo T.A.: Field weakening in buried permanent magnet AC motor drives, IEEE Transactions on Industry Applications, Vol. IA-21,No.2, 1985, pp. 398-407.

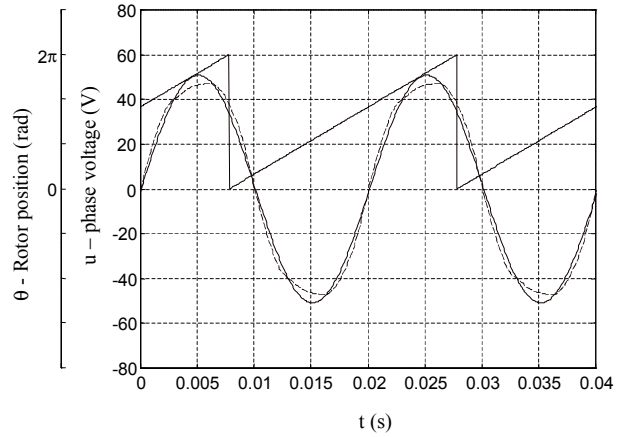

Figuur 6 Rotor position, measured terminal voltage and calculated fundamental voltage for the reference phase of the PMSM (f=50 Hz, 7,6 A, δ=-40,2°).